PERGAMON

International Journal of Heat and Mass Transfer 45 (2002) 2719–2727

International Journal of HEAT and MASS TRANSFER

www.elsevier.com/locate/ijhmt

Shape optimization of rib-roughened surface to enhance turbulent heat transfer

Kwang-Yong Kim *, Sun-Soo Kim

Department of Mechanical Engineering, Inha University, 253, Yonghyun-Dong, Nam-Gu, Inchon 402-751, South Korea

Received 16 February 2001; received in revised form 24 August 2001

Abstract

This work presents an investigation on numerical optimization technique coupled with Reynolds-averaged Navier–Stokes analysis of flow and heat transfer for design of rib-roughened surface in case of single surface roughened in two-dimensional channel. Standard k–ε model is used as a turbulence closure. The objective function is defined as a function of heat transfer coefficient and friction drag coefficient with weighting factor. And, the ratio of width-to-height of the rib and the ratio of pitch-to-height are selected as design variables. Three different weighting factors and two sets of initial values of the design variables in each case are tested. In case of double design variable, the histories of design variables and objective function are complicated, and the number of iterations is very sensitive to the initial values of design variables. However, overall performance of the optimization process is proved quite reliable.

1. Introduction

A popular method to enhance the heat transfer in a flow passage is to roughen the surfaces with discrete square ribs. The applications are found in the design of internal cooling passage of turbine blade, electronic cooling devices, heat exchangers and gas-cooled nuclear reactor fuel pins. However, the surfaces roughened with the ribs cause extra flow resistances. To optimize the shape of rib-roughened surface, thus, it is required to compromise between enhancement of heat transfer and reduction of friction drag.

The performance of the heat transfer surface with square ribs depends significantly on the parameters of the flow structure, such as reattachment length of the separated streamline and turbulence intensities, as well as the area of the surface and Reynolds number. Therefore, shape optimization of the square rib for enhancement of turbulent heat transfer should be based on precise analysis of convective heat transfer. Recently, with the aid of rapid developments of computer technology and numerical algorithms, computational fluid dynamics using Reynolds-averaged Navier–Stokes equations (RANS) has become a practical method for the analysis of complicated turbulent flows and heat transfer. Thus, the optimization based on this higher-level analysis tool is expected to be an efficient and also economic design method for the rib-roughened surface rather than those based on experiments [1] and approximated analysis [2].

Methods for the aerodynamic design optimization have been developed rapidly for the last decade with the aid of high performance computers. The numerical optimization methods [3] are regarded as general design tools with the advantages, such as automated design capability, varieties of constraints, and multidisciplinary applications. The numerical optimization obtains the optimal design by minimization or maximization of objective function without any information of target flowfield. However, due to large computing time, coupling with RANS analysis become practical very recently. These methods with various optimization techniques are being applied widely to the aerodynamic design of airfoils and turbomachinery blades, etc. Application to the

* Corresponding author. Tel.: +82-32-872-3096; fax: +82-32-868-1716.

E-mail address: kykim@inha.ac.kr (K.-Y. Kim).

0017-9310/02/$ - see front matter
PII: S0017-9310(01)00358-1

Nomenclature

c_p	specific heat
$c_{\varepsilon 1}, c_{\varepsilon 2}, c_\mu$	turbulence model constants in k–ε model
D	half height of channel D_h hydraulic diameter
F	objective function
f	friction factor
H	rib height
k	turbulent kinetic energy
L	length of the channel
Nu	Nusselt number
P	production rate of turbulent kinetic energy
PH	pitch-to-height ratio divided by 7.2, Pi/7.2HPi
Pi	rib pitch
Pr, Pr_t	Prandtl number and turbulent Prandtl number
$p, \Delta p$	pressure, pressure drop in a channel
q_0	wall heat flux
Re	Reynolds number
s, s_0	coordinates along surface and of reference point, respectively
T	local mean temperature
$\hat{T}$	transformed mean temperature
U, V	mean velocity components in axial and transverse directions, respectively
$\bar{U}$	average axial velocity
x, y	axial and transverse coordinates, respectively

Greek symbols

β	weighting factor in objective function
ε	dissipation rate of turbulent kinetic energy
v, v_t	molecular and turbulent viscosities, respectively
ρ	fluid density
σ	increasing rate of bulk temperature in axial direction
$\sigma_k, \sigma_\varepsilon$	turbulent Prandtl numbers of k and ε, respectively

heat transfer problems is also expected to be successful, but can be found hardly.

Many experimental and numerical works were carried out to investigate the heat transfer characteristics of rib-roughened surface. Lewis [2] used an analysis based on an approximate model of the separated flow over each roughness element to investigate the performance of a wide range of rough surface. Berger and Hau [4] measured the mass-heat transfer distribution in pipes roughened with small square ribs using an electrochemical analog technique. In this experiment, the rib pitch-to-height ratio, Reynolds number and Schmidt number were varied, and their effects were discussed. Han et al. [1] tested experimentally the effects of rib shape, angle of attack and pitch-to-height ratio on friction factor and heat transfer coefficient. Lau et al. [5] also investigated experimentally the effects of angle of attack on heat transfer coefficient in a wide range of Reynolds number in a squared sectioned duct. The influence of arrangement and length of discrete ribs on heat transfer and friction loss is investigated by Cho et al. [6] with mass transfer experiments. The measurements using laser Doppler velocimetry were reported by Drain and Martin [7]. Computational results with k–ε turbulence model were also obtained and compared with the experimental data. Liou et al. [8] investigated the heat transfer and flow characteristics both numerically and experimentally. They used an algebraic stress turbulence model for the numerical calculations, and adopted a real-time holographic interferometry technique for the experiment. The effects of the flow and geometric parameters on the heat transfer coefficient were discussed. And, the heat transfer correlation was developed in terms of Reynolds number, rib height and rib spacing. In the numerical work of Abdel Gawad [9] for the case with two opposite rib-roughened walls, the effects of the rib height-to-hydraulic diameter ratio and Reynolds number on friction and heat transfer coefficient were investigated, and the effect of rotation was also tested. Recently, the flow and heat transfer on rib-roughened surface was selected as a test case at a ERCOFTAC/IAHR workshop [10], and the performances of various turbulence models were evaluated in comparison with the experimental data. In the results, the v2f model [11] and one of k–ε models with wall function show better predictions of Nusselt number distribution rather than Reynolds stress closures. Although many investigators have studied the effects of geometric parameters of the rib both numerically and experimentally, any of them has not tried to optimize the shape of rib systematically.

The purpose of the present work is to optimize the shape of rib-roughened surface by numerical optimization technique coupled with RANS analysis of flow and heat transfer in case of single surface roughened in two-dimensional channel. The objective function is defined as a linear function of heat transfer coefficient and friction drag coefficient with weighting factor.

2. Numerical analysis

For steady incompressible flow in a two-dimensional channel with periodic ribs mounted on one of the walls, as shown in Fig. 1, Reynolds-averaged equations for mass, momentum and energy conservations in rectangular coordinates, using Boussinesq eddy viscosity hypothesis, can be written as follows:

$$\frac{\partial U}{\partial x}+\frac{\partial V}{\partial y}=0, \tag{1}$$

$$U\frac{\partial U}{\partial x}+V\frac{\partial U}{\partial y}=\frac{\partial}{\partial x}\left[(\nu+\nu_{\mathrm{t}})\frac{\partial U}{\partial x}\right]+\frac{\partial}{\partial y}\left[(\nu+\nu_{\mathrm{t}})\frac{\partial U}{\partial y}\right]-\frac{1}{\rho}\frac{\partial p}{\partial x}, \tag{2}$$

$$U\frac{\partial V}{\partial x}+V\frac{\partial V}{\partial y}=\frac{\partial}{\partial x}\left[(\nu+\nu_{\mathrm{t}})\frac{\partial V}{\partial x}\right]+\frac{\partial}{\partial y}\left[(\nu+\nu_{\mathrm{t}})\frac{\partial V}{\partial y}\right]-\frac{1}{\rho}\frac{\partial p}{\partial y}, \tag{3}$$

$$U\frac{\partial T}{\partial x}+V\frac{\partial T}{\partial y}=\frac{\partial}{\partial x}\left[\left(\frac{\nu}{Pr}+\frac{\nu_{\mathrm{t}}}{Pr_{\mathrm{t}}}\right)\frac{\partial T}{\partial x}\right]+\frac{\partial}{\partial y}\left[\left(\frac{\nu}{Pr}+\frac{\nu_{\mathrm{t}}}{Pr_{\mathrm{t}}}\right)\frac{\partial T}{\partial y}\right]. \tag{4}$$

The bulk temperature increases streamwise due to constant heat flux from the wall. Thus, in order to use the periodic boundary condition, following transformation of the temperature proposed by Webb and Ramadhyani [12] has been employed:

$$T(x,y)=\sigma x+\hat{T}(x,y), \tag{5}$$

where σ is the rate of bulk temperature increase due to wall heat flux, defined as follows:

$$\sigma=\frac{T(x+\mathrm{Pi},y)-T(x,y)}{\mathrm{Pi}}. \tag{6}$$

The rate can be calculated from the heat flux:

$$\sigma=\frac{q_0}{2\rho\bar{U}c_{\mathrm{p}}D}. \tag{7}$$

Then, we can use the following simple periodic boundary condition for temperature:

$$\hat{T}(x,y)=\hat{T}(x+\mathrm{Pi},y). \tag{8}$$

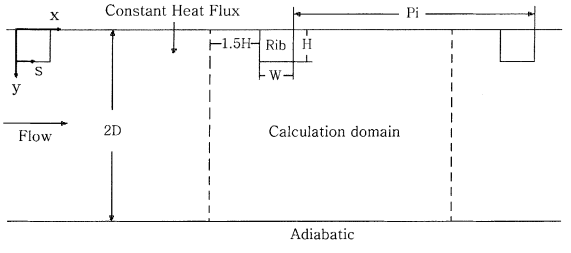

Fig. 1. Flow geometry and calculation domain.

The energy equation (4) is transformed to the following form:

$$U\frac{\partial\hat{T}}{\partial x}+V\frac{\partial\hat{T}}{\partial y}=\frac{\partial}{\partial x}\left[\left(\frac{\nu}{Pr}+\frac{\nu_{\mathrm{t}}}{Pr_{\mathrm{t}}}\right)\frac{\partial\hat{T}}{\partial x}\right]+\frac{\partial}{\partial y}\left[\left(\frac{\nu}{Pr}+\frac{\nu_{\mathrm{t}}}{Pr_{\mathrm{t}}}\right)\frac{\partial\hat{T}}{\partial y}\right]-\sigma U. \tag{9}$$

The turbulent viscosity, ν_{t} is determined by the standard k–ε model [13] as $\nu_{\mathrm{t}}=c_\mu k^2/\varepsilon$, where turbulent kinetic energy, k and its dissipation rate, ε are calculated from the following transport equations:

$$U\frac{\partial k}{\partial x}+V\frac{\partial k}{\partial y}=\frac{\partial}{\partial x}\left[\left(\nu+\frac{\nu_t}{\sigma_k}\right)\frac{\partial k}{\partial x}\right]+\frac{\partial}{\partial y}\left[\left(\nu+\frac{\nu_t}{\sigma_k}\right)\frac{\partial k}{\partial y}\right]+P-\varepsilon, \tag{10}$$

$$U\frac{\partial\varepsilon}{\partial x}+V\frac{\partial\varepsilon}{\partial y}=\frac{\partial}{\partial x}\left[\left(\nu+\frac{\nu_t}{\sigma_\varepsilon}\right)\frac{\partial\varepsilon}{\partial x}\right]+\frac{\partial}{\partial y}\left[\left(\nu+\frac{\nu_t}{\sigma_\varepsilon}\right)\frac{\partial\varepsilon}{\partial y}\right]+c_{\varepsilon1}\frac{\varepsilon}{k}P-c_{\varepsilon2}\frac{\varepsilon^2}{k}, \tag{11}$$

where

$$P=\nu_{\mathrm{t}}\left[\left(\frac{\partial U}{\partial y}+\frac{\partial V}{\partial x}\right)^2+2\left(\frac{\partial U}{\partial x}\right)^2+2\left(\frac{\partial V}{\partial y}\right)^2\right]. \tag{12}$$

The model constants have the following values: $c_\mu=0.09$, $\sigma_k=1.0$, $\sigma_\varepsilon=1.0$, $c_{\varepsilon1}=1.44$, $c_{\varepsilon2}=1.92$, and $Pr_{\mathrm{t}}=0.9$. And, in the near wall region of low-Reynolds number, empirical wall laws have been employed as wall functions.

The governing equations are discretized by finite volume method with power-law scheme. Staggered grids are used. And, the solution procedure is based on SIMPLE algorithm [14].

Considering periodic behavior of the flow, the computational domain of which length is one pitch has been selected as shown in Fig. 1. At the inlet and outlet of the domain, the following periodic conditions are adopted: for each dependent variable except pressure, the inlet value is same as the outlet value at the corresponding transverse location, as Eq. (8) for the transformed temperature. In case of pressure, pressure drop is taken into account. Uniform turbulent kinetic energy is assumed at the inlet as an initial boundary condition. The value is calculated from the following formula: $k=1.5T_{\mathrm{u}}^2U_{\mathrm{b}}^2$, where U_{b} is a bulk velocity of the flow. Turbulent intensity, T_{u} is assumed to be 0.1. Dissipation rate of turbulent kinetic energy is also assumed uniform at the inlet. The value is calculated from the formula: $\varepsilon=c_\mu k^{3/2}/l$, where length scale, l is given as $0.5\times$ (channel height). At the all wall boundaries, the wall function [15] based on empirical wall law is adopted for mean axial velocity.

At the roughened wall, constant heat flux condition is imposed. At the base of the rib, heat flux is constant. At

the variable heat flux boundaries on the rib surfaces, the heat flux distribution is deduced from the empirical data provided by Webb and Ramadhyani [12]. At these boundaries, the wall temperatures are calculated from the empirical wall function [15] and the given wall heat flux.

3. Numerical optimization

In this work, the shape of the roughened surface has been optimized numerically to maximize the performance. The present numerical optimization problem is defined as minimization of an objective function $F(\mathbf{x})$ with $x_i^{\mathrm{l}} \leqslant x_i \leqslant x_i^{\mathrm{u}}$, where $\mathbf{x}$ is a vector of design variables, and x_i^{l} and x_i^{u} are lower and upper bounds of each design variable.

The search direction is initially found by the steepest decent method [16]. But, subsequent procedure is repeated by the conjugate direction method. The golden section method is used to determine the optimum moving distance along the search direction. The same optimization algorithms have been used to design the blade of an axial-flow compressor [16]. In general gradient-based optimization method such as used in this work, the direction is calculated from the gradients of objective function. Convergence criterion is also based on the norm of gradient of objective function. Fig. 2 shows flow chart of the present optimization process.

The geometric variables of the two-dimensional channel with singled surface roughened, shown in Fig. 1,

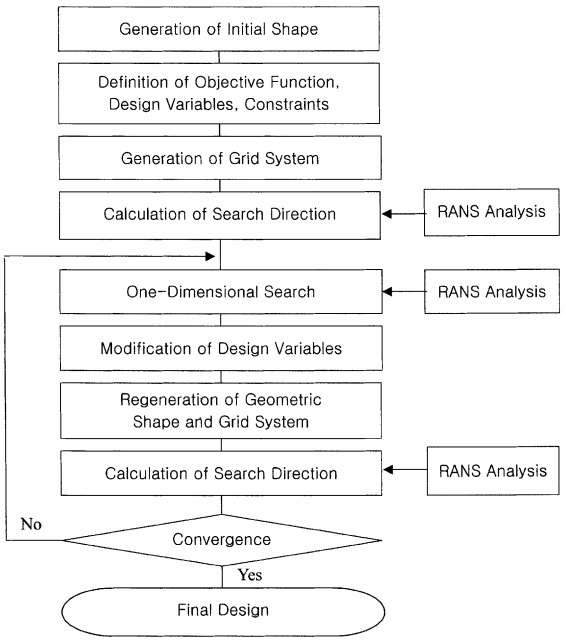

Fig. 2. Optimization process.

are height of the channel (2D), height of the rib (H), width of the rib (W) and pitch of the periodic ribs (Pi). Therefore, three dimensionless geometric variables are found: D/H, W/H and Pi/H. In this work, the ratio of width-to-height of the rib (W/H) and the ratio of pitch-to-height of the rib (Pi/H) are selected as design variables with fixed D/H.

The ribs on the surface are introduced to increase the heat transfer, but inevitably cause extra flow resistances. Thus, to maximize the performance of the ribs, the optimum shape should be determined by compromising between the enhancement of heat transfer and reduction of friction loss. On this purpose, the objective function is defined as follows:

$$F = F_{Nu} + \beta F_f. \tag{13}$$

The first term on the right-hand side is defined as an inverse of Nusselt number:

$$F_{Nu} = \frac{1}{Nu_a}, \tag{14}$$

where

$$Nu_a = \frac{\int_{s_0}^{s_0+\mathrm{Pi}+2H} Nu/Nu_{\mathrm{s}}\,\mathrm{d}s}{\mathrm{Pi}+2H},$$

$$Nu_{\mathrm{s}} = 0.023 Re^{0.8} Pr^{0.4},$$

Nu_{s} is the Nusselt number obtained from the Dittus–Boelter correlation, which is for the fully developed turbulent flows in a smooth pipe.

The second term in Eq. (13) is related to the friction loss, and is defined as follows:

$$F_f = \left(\frac{f}{f_0}\right)^{1/3}, \tag{15}$$

where

$$f = \frac{\Delta p D_h}{2\rho \bar{U}^2 L},$$

$$f_0 = 2(2.236 \ln Re - 4.639)^{-2},$$

f_0 is a friction factor for fully developed flow in a smooth pipe, and is obtained from Petukhov empirical correlation [17] which is modified from the Karman–Nikuradse correlation for the best fit in the range, $10^4 < Re < 10^6$. In the optimization, this term acts like a penalty function to prevent excessive friction loss. The weighting factor, β is adjusted to the purpose by the designer.

4. Results and discussion

4.1. Flow analysis

The test flow for the numerical analysis is same as that measured by Drain and Martin [7] (Fig. 1), where

heights of the channel (2D) and the rib (H) are 0.04 and 0.008 m, respectively, with $W/H = 1.0$ and $\mathrm{Pi}/H = 7.2$. For the validation of numerical solution of the velocity field, the results are compared with the experimental data measured by Drain and Martin [7], of which Reynolds number is 37,200. On the other hand, the computational results for the distribution of Nusselt number are validated based on the measurements of Liou et al. [8], which were obtained by holographic interferometry technique at Reynolds number, 12,600.

Grid dependency tests are carried out to find an optimum grid. Three different grids, 42×31, 62×41 and 82×51 are tested. As shown in Fig. 3, grid-independent solutions are obtained only with the finer grids, 62×41 and 82×51. Thus, 62×41 grid is selected as an optimum grid, which is denser near the wall. Fig. 4 shows streamlines of the flowfield. A smaller recirculation due to adverse pressure gradient and separation/reattachment with a larger recirculation are found upstream and downstream of the rib, respectively. Isothermal contours are shown in Fig. 5. Since the temperatures are those transformed by Eq. (5), there is no inclination of isothermal lines in free stream.

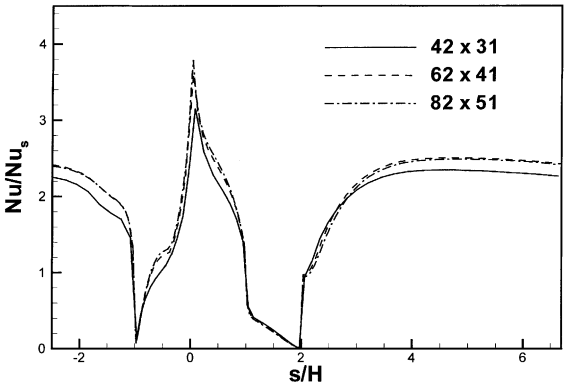

Fig. 3. Grid dependency test – local Nusselt number distributions ($Re = 12{,}600$).

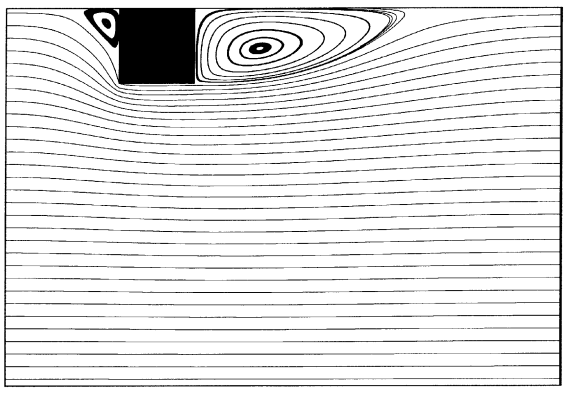

Fig. 4. Streamlines ($Re = 37{,}200$).

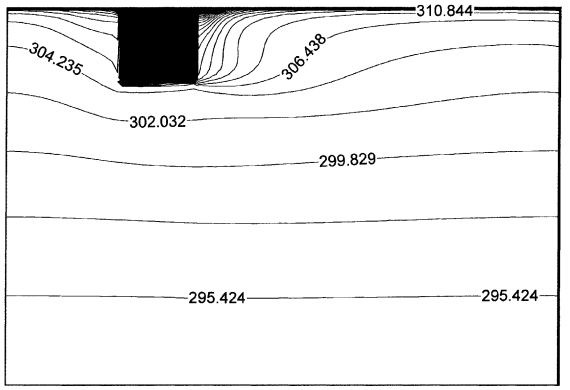

Fig. 5. Temperature contours ($Re = 12{,}600$).

The computed profiles of mean axial velocity are compared with empirical profiles in Fig. 6. At $x/H = 4.18$, the computed profile indicates that the flow is already in the redevelopment region near the upper wall, while the measurements are still in separation region. Maximum velocities are generally overestimated, and its locations are shifted to the smooth wall. The discrepancies seem to result from the well-known defects of standard k–ε model and conventional wall-laws in the recirculation region. However, the results are very similar to those obtained with an algebraic stress model by Liou et al. [8], qualitatively and also quantitatively.

The distributions of local Nusselt number are compared in Fig. 7. The values are underestimated on the surfaces of the rib, especially on the sides, probably due to the approximation of heat flux distribution on the rib surfaces. And, the values are overestimated just downstream of the rib, which results from the underestimation of reattachment length. Although the agreement with experimental data is not excellent, it is sufficient for

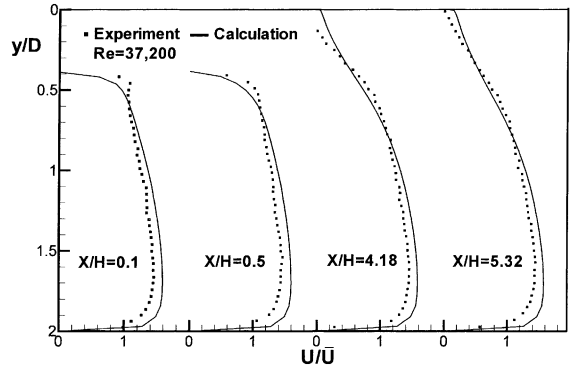

Fig. 6. Comparison of predicted and measured mean velocity profiles ($Re = 37{,}200$).

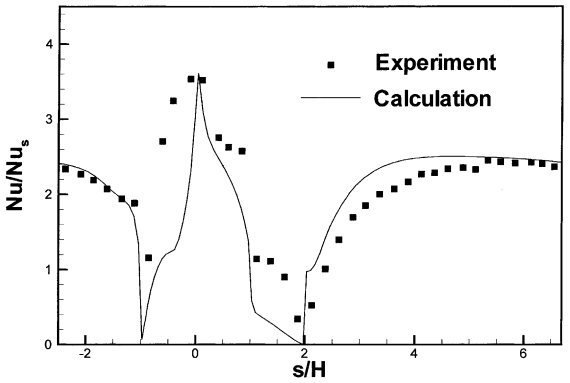

Fig. 7. Comparison of predicted and measured local Nusselt number distributions ($Re = 12{,}600$).

the purpose of present optimization. Since only the average level of Nusselt number is concerned in the present optimization problem, the discrepancies in the Nu distribution, not in the average level, are expected not to be large influence on the results of the optimization.

From the distribution of Nusselt number, enhancement of heat transfer is expected by reducing the reattachment length. As shown in Fig. 8, there is an optimum value of Pi/H which gives the maximum average Nusselt number (Nu_a), since increase of Pi/H reduces the separation region, but, also reduces the turbulent intensity which promotes turbulent heat transfer. It is interesting to note that friction factor has also a maximum value near Pi/7.2H = 1.5. Han et al. [1] concluded, from their experimental results with symmetric and staggered ribs, that friction factor has a maximum value when the pitch-to-height ratio of the rib is approximately 10. This is consistent with the present result, even though the cases are different. Fig. 9 shows that increase of W/H decreases the heat transfer, but decreases the friction loss, either.

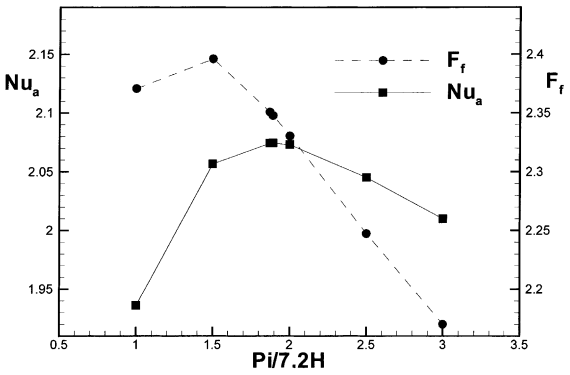

Fig. 8. Effects of Pi/H on Nusselt number and friction factor with $W/H = 1.0$ ($Re = 12{,}600$).

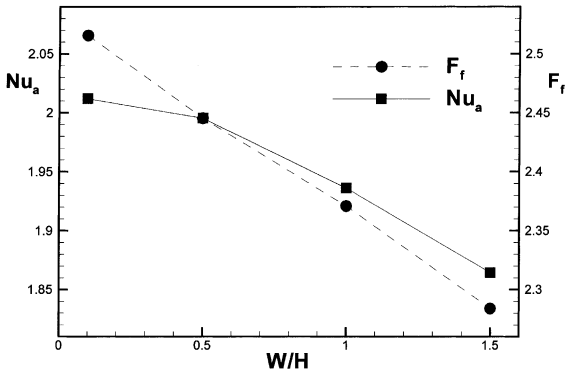

Fig. 9. Effects of W/H on Nusselt number and friction factor with $PH = 1.0$ ($Re = 12{,}600$).

4.2. Numerical optimization

Initial flow and heat transfer conditions for the present optimizations are same as those of the experiment by Liou et al. [8]. Thus, the Reynolds number for the optimizations is 12,600. The optimum shape and distribution of the ribs on the surface are determined by minimization of the objective function. The computational grid is modified automatically with the change of geometric design variables. An algebraic stretching method is employed to modify grid spaces and length of the computational domain. Since the number of grids is fixed throughout the calculations, the stretching factor is adjusted to the change of design variables. The whole computational domain is divided into three regions: upstream, downstream and rib regions. In the region upstream of the rib (Fig. 1), the value of stretching factor is fixed. But, in the rib and downstream regions, the values are determined to be proportional to the values of design variables, W/H and PH, respectively.

Since the objective function is less sensitive to Pi/H, this variable is replaced by PH (= Pi/7.2H) of which scale is equivalent to that of W/H. The minimum number of iterations is set to be five. The results of optimizations for all the test cases are summarized in Table 1. Three different values of the weighting factor in definition of objective function (Eq. (13)), i.e. 0.0, 0.05 and 0.1 are tested.

When the weighting factor is 0.0, the objective function is defined only in terms of Nusselt number. As already mentioned, decrease of W/H increases monotonically the heat transfer, while there is an optimum value of PH. In any case, minimum objective function is obtained when W/H approaches zero. Therefore, in this case, only PH is used as a design variable. Two different values of W/H, 0.01 and 1.0 are tested. $W/H = 0.01$ is regarded as a minimum value since zero width of the rib results in computational failure. In cases of weighting factor, 0.05 and 0.1, three different sets of design

Table 1
Results of numerical optimizations

Optimization case		Initial value		Final value		No. of flow analyses	No. of design variable changes
β	Design variable	Design variable	Objective function	Design variable	Objective function		
0.0	PH $(W/H = 0.01)$	1.0	0.4547746	1.4302030	0.4428154	70	5
		3.0	0.4805100	1.4585218	0.4427826	92	5
	PH $(W/H = 1.0)$	1.0	0.5165296	1.8838503	0.4820777	85	5
		3.0	0.4975415	1.8815553	0.4820769	80	5
0.05	PH $(W/H = 1.0)$	1.0	0.6350319	2.0783792	0.5987008	131	7
		3.0	0.6060246	2.0794742	0.5987080	133	7
	W/H $(PH = 1.0)$	0.5	0.6233899	0.2557926	0.6195324	88	5
		0.2	0.6198785	0.2469523	0.6195540	77	5
	PH–W/H	2.0–0.5	0.5927094	2.1414368–0.1075294	0.5877771	1185	60
		1.5–1.0	0.6060225	2.1891468–0.1060136	0.5877553	353	14
0.1	PH $(W/H = 1.0)$	1.0	0.7535788	2.5675297	0.7136303	101	5
		3.0	0.7145299	2.5512712	0.7136117	130	7
	W/H $(PH = 1.0)$	0.1	0.7486252	0.2981259	0.7436907	82	5
		1.0	0.7535788	0.2965683	0.7437022	95	5
	PH–W/H	1.0–1.0	0.7535788	2.7439132–0.3050597	0.7052742	627	28
		1.5–1.0	0.7258314	2.7777777–0.3043487	0.7052715	139	6

variables are tested in each case: PH with $W/H = 1.0$, W/H with $PH = 1.0$, and both of PH and W/H. Therefore, total eight different cases are tested as shown in Table 1. In each case, optimizations are performed with two different sets of initial values to confirm the optimum point. The maximum relative error of the minimum objective function is less than 0.01%. However, for the optimum design variables, the maximum relative error is 3.5% in case with $\beta = 0.05$ and W/H as design variable, followed by 2.2% in case with $\beta = 0.05$ and $W/H - PH$ as design variables. In all the remaining cases, the relative errors are less than 2.0%. The errors can be attributed to the numerical instabilities, but also depends on the convergence criteria of the optimization process. It is possible to estimate approximately the total computational time of the optimization process with "no. of flow analyses" in Table 1 which means the total number of flow analyses required throughout the optimization process.

In case with zero weighting factor and $W/H = 1.0$, the optimum PH is about 1.88, which corresponds to $\mathrm{Pi}/H = 13.5$. Liou et al. [8] presented a correlation for average Nusselt number in terms of Pi/H, Re and the ratio of H to hydraulic diameter, based on their numerical calculations. The present result for optimum Pi/H is consistent with this correlation within the error bounds.

Figs. 10–12 show histories of objective function and design variables in optimization processes. The histories

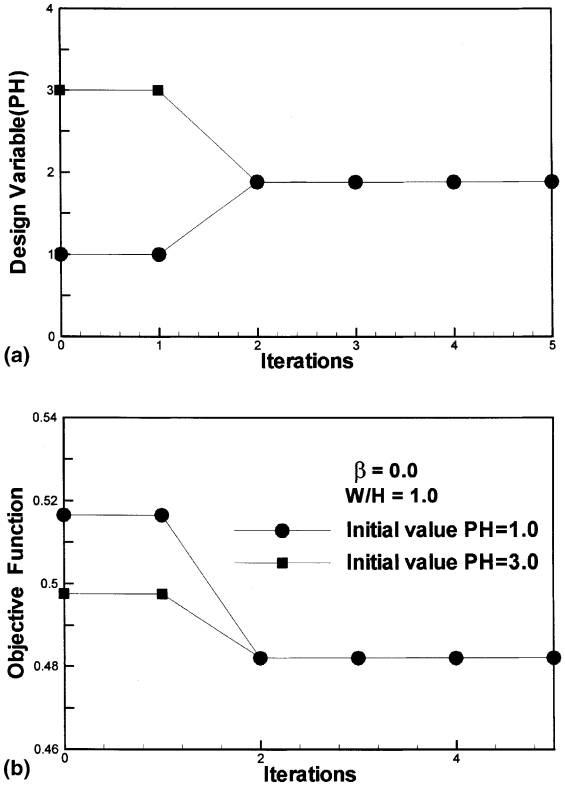

Fig. 10. Histories of design variable and objective function with $\beta = 0.0$ and $W/H = 1.0$.

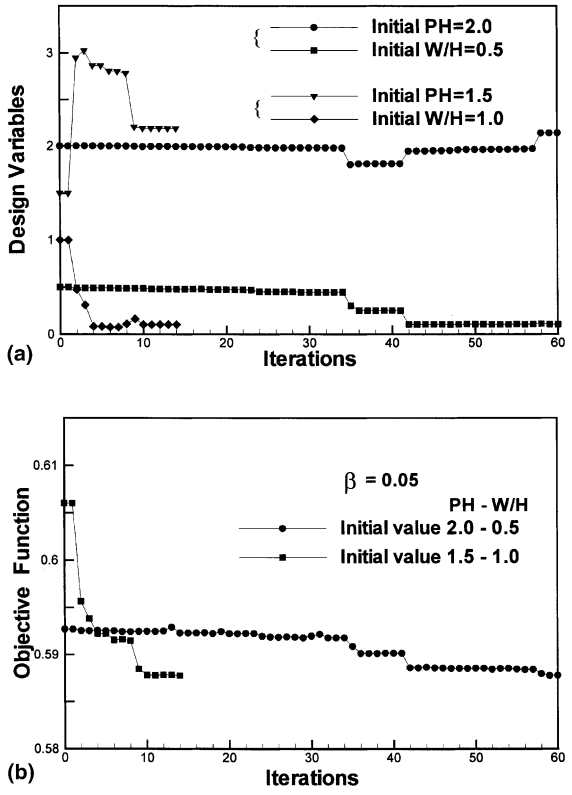

Fig. 11. Histories of two design variables and objective function with $\beta = 0.05$.

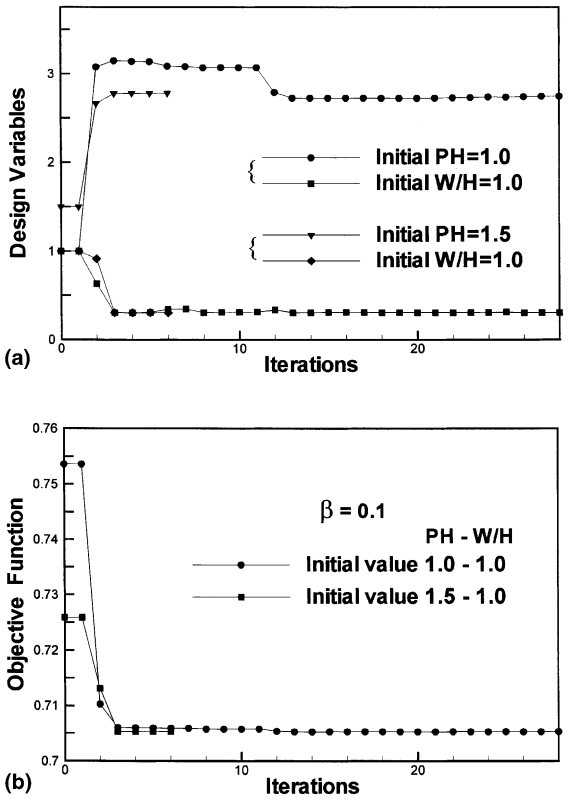

Fig. 12. Histories of two design variables and objective function with $\beta = 0.1$.

in the case with $\beta = 0.0$ and $W/H = 1.0$ are shown in Fig. 10. In this case of single design variable, the process finds effectively the almost optimum value at second iteration, and reaches the final value within 5th iteration, regardless of initial value. Both Figs. 11 and 12 show the histories in case of double design variables. For example, in Fig. 11(a), ▼ and ◆ indicate the histories of design variables, PH and W/H, respectively, in case with initial values, $PH = 1.5$ and $W/H = 1.0$. It is found in these figures that the histories are complicated, and that the number of iterations, i.e. the maximum number of design variable changes required to converge the optimization process, is very sensitive to the initial values of design variables. In the case with $\beta = 0.05$, shown in Fig. 11, more than five times larger number of iterations is required with different set of initial values. It does not seem that the number of iterations reduces as the initial values of the design variables approach the final values. Thus, it is difficult to find the general way to optimize the computing time.

Since the heat transfer and the friction loss depend on Reynolds number, it is expected that the optimum shape of the rib also depends on the Reynolds number. Thus, the influence of Reynolds number on an optimum design variable has been examined for a sample case (single design variable, W/H with $PH = 1.0$ and $\beta = 0.05$), and the results are presented in Fig. 13, where the optimum value of the design variable is influenced by the Reynolds number as expected, but only slightly.

The computations were carried out by the personal computer with Intel Pentium III CPU, using MS-

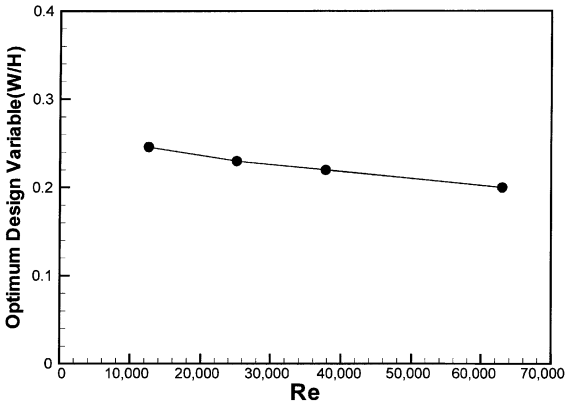

Fig. 13. Effect of Reynolds number on the optimum design variable, W/H with $PH = 1.0$ and $\beta = 0.05$.

Developer Studio Ver. 6.0 as program compiler. The computing time of single flow analysis is in the range 10–15 min.

5. Conclusions

The shape of rib-roughened surface has been optimized by numerical optimization technique coupled with RANS analysis of flow and heat transfer. Computed reattachment length is shorter than the measurement. Discrepancies are also found on the surfaces of the rib, which probably result from the approximation of heat flux distribution. However, the analysis gives generally good prediction enough to estimate the overall heat transfer performance of specific rib shape. The objective function is designed so as to maximize the performance of the ribs by compromising between enhancement of heat transfer and reduction of friction loss. And, the ratio of width-to-height of the rib and the ratio of pitch-to-height are selected as design variables. In case single design variable, the process finds very effectively the optimum value within 5th iteration, regardless of initial value. However, in case of double design variable, the histories of design variables and objective function are complicated, and the number of iterations is very sensitive to the initial values of design variables. The maximum relative error of the minimum objective function with two different sets of the initial values, however, is less than 0.01%, while that of the optimum design variables is less than 2.0% in most of the cases. The optimum value of design variable is influenced slightly by the Reynolds number. As the conclusion, the numerical optimization with RANS analysis is validated as a promising tool for design of heat transfer surface. Further researches to reduce the computing time and to improve the accuracy of the analysis are being required.

References

[1] J.C. Han, L.R. Glicksman, W.M. Rohsenow, An investigation of heat transfer and friction for rib-roughened surface, Int. J. Heat Mass Transfer 21 (1978) 1143–1156.

[2] M.J. Lewis, Optimising the thermohydraulic performance of rough surfaces, Int. J. Heat Mass Transfer 18 (1975) 1243–1248.

[3] G.N. Vanderplaats, Numerical Optimization Techniques for Engineering Design with Applications, McGraw-Hill, New York, 1984.

[4] F.P. Berger, K.-F. Hau, F.-L. Hau, Local mass/heat transfer distribution on surface roughened with small square ribs, Int. J. Heat Mass Transfer 22 (1979) 1645–1656.

[5] S.C. Lau, R.D. McMillin, J.C. Han, Turbulent heat transfer and friction in a square channel with discrete rib turbulators, ASME J. Turbomach. 113 (1991) 360–366.

[6] H.H. Cho, S.J. Wu, H.J. Kwon, Local heat/mass transfer measurements in a rectangular duct with discrete ribs, ASME J. Turbomach. 122 (2000) 579–586.

[7] L.E. Drain, S. Martin, Two-component velocity measurements of turbulent flow in a ribbed-wall flow channel, in: International Conference on Laser Anenometry – Advanced and Application, 1985, pp. 99–112.

[8] T.M. Liou, J.J. Hwang, S.H. Chen, Simulation and measurement of enhanced turbulent heat transfer in a channel with periodic ribs on one principal wall, Int. J. Heat Mass Transfer 36 (1993) 507–517.

[9] A.F. Abdel Gawad, Calculation of turbulent flow through a channel with two opposite ribbed-walls, ASME FEDSM2000-11180, 2000.

[10] T. Craft (Ed.), Two-dimensional flow and heat transfer over a smooth wall with square sectioned ribs, in: Proceedings of the Seventh ERCOFTAC/IAHR Workshop on Refined Turbulence Modelling, Test Case 7.2, 1998. Available from http://tmdb.ws.tn.tudelft.nl/workshop7/case7_2/case72d.html.

[11] P. Durbin, Separated flow computations with the k–ε-v^2 model, AIAA J. 33 (1995) 659–664.

[12] B.W. Webb, S. Ramadhyani, Conjugate heat transfer in a channel with staggered ribs, Int. J. Heat Mass Transfer 28 (1985) 1679–1687.

[13] B.E. Launder, D.B. Spalding, The numerical computation of turbulent flows, Comput. Meth. Appl. Mech. Eng. 3 (1974) 269–289.

[14] S.V. Partankar, Numerical Heat Transfer and Fluid Flow, McGraw-Hill, New York, 1980.

[15] K.Y. Kim, Y.J. Lee, Prediction of turbulent heat transfer downstream of an abrupt pipe expansion, KSME Int. J. 8 (1994) 248–254.

[16] S.Y. Lee, K.Y. Kim, Design optimization of axial flow compressor blades with three-dimensional Navier–Stokes solver, KSME Int. J. 14 (2000) 1005–1012.

[17] B.S. Petukhov, in: Advances in Heat Transfer, vol. 6, Academic Press, New York, 1970, pp. 503–504.